Article

Not peer-reviewed version

Contrasting Effects of Bi and Si Substitution at the Ni Site on Magnetostructural Transitions and Magnetocaloric Properties in Ni–Mn–In Heusler Alloys

Abhiyan Oli * , Igor Dubenko , Alexander Granovsky , Dushmantha K Gusthigngnhadurage , Muhammad Abdullah Iqbal , Margaret P Hill , Shane Stadler , Naushad Ali , Saikat Talapatra

Posted Date: 10 April 2026

doi: 10.20944/preprints202604.0708.v1

Keywords: rare-earth-free alloy; heusler alloys; magnetocaloric effect; magnetic entropy change; relative cooling power; magnetic refrigeration

Article

Contrasting Effects of Bi and Si Substitution at the Ni Site on Magnetostructural Transitions and Magnetocaloric Properties in Ni–Mn–In Heusler Alloys

Abhiyan Oli [1,*], Igor Dubenko [1], Alexander Granovsky [2,3,4], Dushmantha K Gusthigngnhadurage [1], Muhammad Abdullah Iqbal [1], Margaret P Hill [5], Shane Stadler [6], Naushad Ali [1] and Saikat Talapatra [1]

[1] School of Physics and Applied Physics, Southern Illinois University, Carbondale, USA
[2] Faculty of Physics, Lomonosov Moscow State University, Moscow, Russia
[3] Samarkand State University, 140104 Samarkand, Uzbekistan
[4] Institute for Theoretical and Applied Electrodynamics RAS, 125412 Moscow, Russia
[5] Department of Chemistry & Physics, Southeast Missouri State University, Cape Girardeau, USA
[6] Department of Physics & Astronomy, Louisiana State University, Baton Rouge, USA
* Correspondence: abhiyan.oli@siu.edu

Abstract

We investigated the structural, magnetic, magnetocaloric, and magnetotransport properties of $Ni_{50}Mn_{35}In_{15}$ Heusler alloys by partial substitution of Ni with 3 at.% Bi ($Ni_{47}Bi_3Mn_{35}In_{15}$) and Si ($Ni_{47}Si_3Mn_{35}In_{15}$) synthesized by arc-melting. X-ray diffraction confirms a predominant $L2_1$ cubic structure (space group Fm-3m), while SEM/EDX verifies compositional homogeneity. Temperature-dependent magnetization measurements reveal that the Bi-substituted alloy exhibits a first-order magnetostructural transition associated with the martensitic transformation, followed by a second-order ferromagnetic–paramagnetic transition near the Curie temperature. In contrast, the Si-substituted alloy shows a single second-order transition with negligible thermal hysteresis, indicating suppression of the martensitic phase. The Curie temperature decreases from 324 K for the parent alloy to 313 K and 286 K for the Bi- and Si-substituted alloys, respectively. A maximum magnetic entropy change of 6.0 $Jkg^{-1}K^{-1}$ and 4.5 $Jkg^{-1}K^{-1}$ is obtained under an applied magnetic field change of 50 kOe for the Bi- and Si-substituted alloys, respectively, with corresponding relative cooling power values of 303 Jkg^{-1} and 345 Jkg^{-1}.These results demonstrate that lattice expansion (Bi) and contraction (Si) distinctly modify Mn–Mn exchange interactions, enabling tunable magnetocaloric performance in Ni–Mn–In Heusler alloys.

Keywords: rare-earth-free alloy; heusler alloys; magnetocaloric effect; magnetic entropy change; relative cooling power; magnetic refrigeration

Introduction

Magnetic refrigeration is an emerging sustainable cooling technology with significant potential to reduce greenhouse gas emissions and mitigate global warming. This approach offers higher energy efficiency compared to conventional vapor-compression refrigeration systems [1–3]. The performance of magnetic refrigeration is governed by the magnetocaloric effect (MCE), which refers to the reversible temperature change of a magnetic material upon the application and removal of an external magnetic field, resulting in heating during magnetization and cooling during demagnetization [4,5]. Researchers have identified several materials that are nearly suitable for

 doi:10.20944/preprints202604.0708.v1

magnetic cooling systems. While Gd-based magnetic materials have shown promising properties, their high cost and limited availability hinder large-scale practical applications, leading to the search for alternative materials [6–8]. In this regard, Ni-Mn-In based Heusler alloys have emerged as promising candidates due to their tunable magnetostructural transitions and significant magnetocaloric response. Heusler alloys are a class of intermetallic compounds composed of combinations of transition elements and one or more sub-group elements. They can be classified into different types based on their general formulas such as X_2YZ, XYZ, Y_2XZ, XX`YZ (where X and Y are typically 3d transition elements and Z is a main-group element such as Al, In, Ga, Si, or Sb) termed as full, semi, inverse, and quaternary Heusler alloys, respectively [9,10]. Research into off-stoichiometric Ni-Mn-In-based Heusler alloys has been particularly attractive because of their remarkable magneto-responsive properties including magnetic shape memory effects, large magnetoresistance, anomalous Hall effect, and both normal and inverse magnetocaloric effects [11–14].

Previous studies have shown that off-stoichiometric Ni-Mn-In based alloys undergo structural transitions from a high-temperature austenitic phase (AP) to low-temperature martensitic phase (MP) near room temperature. Additionally, they undergo magnetic phase transitions from antiferromagnetic (AFM) to a ferromagnetic (FM) phase around the martensitic temperature (T_M), and from FM to paramagnetic (PM) around the Curie temperature (T_C) [15–17]. The crystal structure of the alloy is temperature-dependent and can transition between a high-temperature AP, a low-temperature MP, and mixed phases near the temperature-induced structural (martensitic) transition ($T=T_M$ (T_A)), where T_M and T_A are the forward and reverse transition temperatures, respectively [18,19]. In their austenitic phase, full-Heusler alloys crystallize in an $L2_1$ cubic phase, while semi-Heusler compounds crystallize in a $C1_\beta$ phase. Substitution at the Ni site in $Ni_{50}Mn_{35}In_{15}$- based alloys can significantly alter their physical properties. Such substitution modifies the conduction electron concentration (e/a ratio), Mn–Mn interatomic separation, and 3d–3d hybridization, thereby tuning the electronic, magnetic, and structural behavior of the system [15,20].

A.K. Pathak et al. [21] investigated the magnetocaloric effect (MCE) in $Ni_{50}Mn_{34}In_{16}$ and reported a maximum magnetic entropy change ($|\Delta S_M|$) of $\approx$ 6.8 $Jkg^{-1}K^{-1}$ near the Curie temperature (T_C = 325 K) and 5.3 $Jkg^{-1}K^{-1}$ around T_M $\approx$ 280 K under an applied field change of ΔH = 50 kOe. In another study, L. Chen et al. [22] examined $Ni_{45}Co_{4.75}Fe_{0.25}Mn_{36.6}In_{13.4}$ which exhibited a significantly higher $|\Delta S_M|$ of 25 $Jkg^{-1}K^{-1}$ at 281 K under ΔH = 5T. Stadler et al. [19] reported an exceptionally large magnetic entropy change of 65 $Jkg^{-1}K^{-1}$ and a relative cooling power (RCP) of 72 J kg^{-1} in $Ni_2Mn_{0.75}Cu_{0.25}Ga$ near $T_C \approx$ 310 K. Furthermore, Bourgault et al. [23] observed a $|\Delta S_M|$ of 20 J kg^{-1} K^{-1} with a higher RCP of 220 J kg^{-1} in $Ni_{45}Co_5Mn_{37.5}In_{12.5}$ around $T_C \approx$ 368 K.

The Heusler alloys $Ni_{50}Mn_{50-x}In_x$ (x = 15, 15.05, 15.2, 16) [21], are reported to exhibit a gradual increase in $|\Delta S_M|$ and a significant enhancement in RCP near T_C with increasing In concentration. In the case of $Ni_{50}Mn_{35}In_{15-x}Bi_x$ (x = 0, 0.25, 0.5, 1.5), the saturation magnetization and magnetic entropy change (ΔS_M) decrease with increasing x, while the RCP increases [18]. Additionally, substitution of Bi at the Ni site in $Ni_{49}BiMn_{35}In_{15}$ has been reported to yield enhanced $|\Delta S_M|$ and RCP compared to the parent alloy $Ni_{50}Mn_{35}In_{15-x}Bi_x$ ($x \geq 0.5$) [15]. These studies demonstrate that compositional tuning significantly influences magnetocaloric performance; however, a direct comparison of contrasting substitutions (such as Bi and Si) at the Ni site remains limited.

Previous studies have shown that introducing Bi into such alloys decreases the martensitic transition temperature (T_M) while enhancing magnetization, magnetic entropy change (ΔS_M), and relative cooling power (RCP) [15,18]. These effects are highly desirable for magnetic refrigeration applications. Despite these advances, the impact of higher substitution levels on the Ni site remains insufficiently explored. In particular, the $Ni_{47}Bi_3Mn_{35}In_{15}$ (Ni-Bi) composition is of particular interest, as it involves a relatively higher level of Bi substitution (3 at.%) at the Ni site, representing a compositional regime that remains largely unexplored in the literature. Likewise, the $Ni_{47}Si_3Mn_{35}In_{15}$ (Ni-Si) alloy enables a systematic comparison, allowing direct evaluation of the contrasting effects of

 doi:10.20944/preprints202604.0708.v1

lattice expansion (Bi) and lattice contraction (Si) on the structural, magnetic, magnetocaloric, and magnetotransport properties.

Experimental Methods

Pure elements Ni, Bi, Si, In, and Mn with a purity of no less than 99.99%, were used to prepare $Ni_{47}Bi_3Mn_{35}In_{15}$ and $Ni_{47}Si_3Mn_{35}In_{15}$ alloys with a total mass of about 5g. Excess Mn by about 5% was added to compensate for possible mass loss during arc melting. The elements were weighed accurately to match the desired chemical composition and arc-melted under a flow of ultra-high purity argon gas. The resulting ingots were re-melted three or four times to ensure homogeneity. This ingot was then cut into small pieces for magnetization and resistivity measurements and ground into powder for structural analysis. The sample purity and crystal structure were characterized using powder x-ray diffraction (XRD) with Cu- kα radiation (λ = 1.5406 Å) at room temperature, with a step size of 0.012°/step. To confirm the homogeneity of the alloys, scanning electron microscopy (SEM) and energy-dispersive X-ray spectroscopy (EDX) were performed using a Quanta 450 FEG scanning electron microscope equipped with an Oxford Instruments X-Max 50 EDX detector.

Magnetization and resistivity measurements were conducted using a superconducting quantum interference device (SQUID MPMS, Quantum Design, USA). The temperature-dependent magnetization was measured over the range of 10 – 380 K during both heating and cooling cycles under applied magnetic fields of 100 Oe and 50 kOe. Field-dependent isothermal magnetization curves were used to calculate the magnetic entropy change (ΔS_M) by applying a Maxwell relation: $|\Delta S_M| = \int_{H1}^{H2} \left(\frac{dM}{dT}\right)_H dH$, where H_1 and H_2 are initial and final magnetic fields.

The relative cooling power (RCP) was calculated using RCP = $|\Delta S_M|$ x δT_{FWHM}, where δT_{FWHM} is the full-width-at-half-maximum of the $|\Delta S_M|$ curve. The Refrigerant capacity (RC) was determined using $RC = \int_{T_1}^{T_2} |\Delta S_M(T)| dT$, where T_1 and T_2 are temperature corresponding to the half-maximum points of the $|\Delta S_M|$ peak [11].

Results and Discussion

Figure 1 (a) presents the room-temperature X-ray diffraction (XRD) patterns of $Ni_{47}Bi_3Mn_{35}In_{15}$ and $Ni_{47}Si_3Mn_{35}In_{15}$, confirming that both compounds crystallize in a face-centered cubic (fcc)-like structure with space group Fm-3m ($L2_1$ ordered phase) [24]. A decrease in lattice parameter is observed from 6.015 Å for the Ni-Bi alloy to 5.997 Å Ni-Si alloy, which can be attributed to the smaller atomic radius of Si compared to Bi. The observed variation in lattice parameter directly influences the Mn–Mn interatomic distance, which plays a crucial role in governing the magnetic exchange interactions in these alloys. For comparison, the parent alloy $Ni_{50}Mn_{35}In_{15}$, has been reported to exhibit a lattice parameter of a = 5.884 Å with a mixed-phase structure [18], while $Ni_{49}BiMn_{35}In_{15}$ exhibits a = 5.926 Å [15]. The inset of Fig. 1(a) shows the variation of lattice parameter for $Ni_{50-x}Bi_xMn_{35}In_{15}$ (x = 0,1,3), demonstrating a systematic increase with increasing Bi concentration, consistent with lattice expansion due to the larger atomic size of Bi relative to Ni. Additional diffraction peaks are observed in the Bi-containing samples, which may indicate the presence of minor secondary phases, possibly due to Bi segregation. Furthermore, slight shifts and broadening of the main peaks suggest possible structural instability, which may indicate the proximity of a martensitic transformation near room temperature. However, temperature-dependent XRD measurements are required to definitively confirm this behavior [21,25].

Preprints.org (www.preprints.org) | NOT PEER-REVIEWED | Posted: 10 April 2026 doi:10.20944/preprints202604.0708.v1

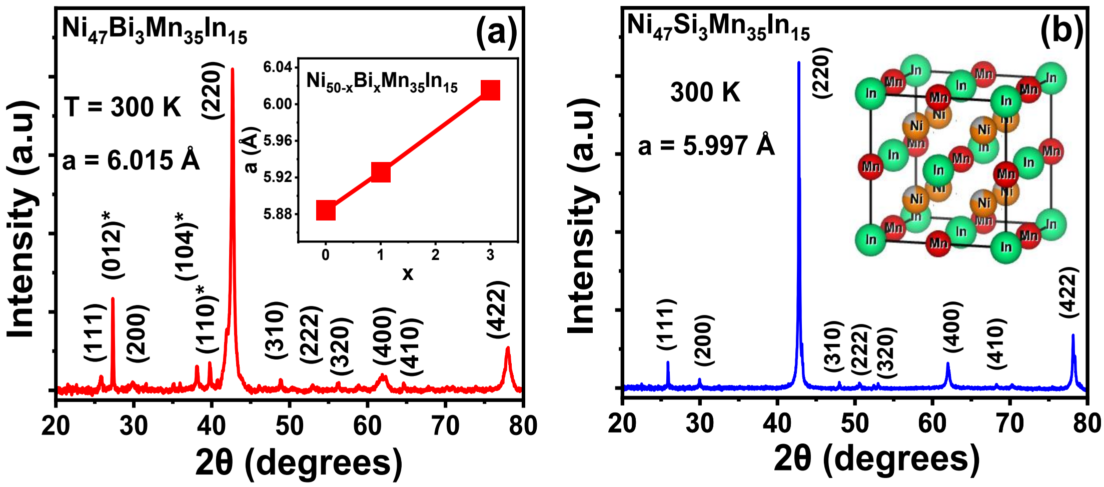

Figure 1. Room-temperature X-ray diffraction (XRD) patterns of (a) $Ni_{47}Bi_3Mn_{35}In_{15}$ and (b) $Ni_{47}Si_3Mn_{35}In_{15}$ alloys. The asterisk (*) in panel (a) denotes secondary phases associated with Bi. The inset in (a) shows the variation of lattice parameter for $Ni_{50-x}Bi_xMn_{35}In_{15}$ (x = 0,1,3). The inset in (b) shows the $L2_1$ cubic unit cell of the Ni-Mn-In based Heusler alloy.

In Figure 2, panel (a) and (b) present the SEM micrographs and corresponding EDX analyses of $Ni_{47}Bi_3Mn_{35}In_{15}$ and $Ni_{47}Si_3Mn_{35}In_{15}$, respectively, to examine their surface morphology and elemental composition. The SEM images reveal relatively uniform and homogeneous microstructures without noticeable phase segregation, while the corresponding EDX spectra confirm the presence of all constituent elements. Table 1 compares the nominal and experimentally obtained weight percentages from EDX analysis, showing good agreement within ~5% deviation, consistent with the typical accuracy of EDX measurements. Minor deviations are observed, which can be attributed to the surface-sensitive nature of EDX, possible carbon coating, slight oxidation, and the intentional addition of excess Mn to compensate for evaporation losses during arc melting [25]. Overall, the close agreement between measured and nominal compositions confirms the successful formation of the target alloys and demonstrates good chemical homogeneity and the reliability of the synthesis process.

Table 1. Comparison of nominal (Exp. Wt.%) and experimentally obtained (EDX Wt.%) weight percentages from EDX analysis for (a) $Ni_{47}Bi_3Mn_{35}In_{15}$ and (b) $Ni_{47}Si_3Mn_{35}In_{15}$.

$Ni_{47}Bi_3Mn_{35}In_{15}$				$Ni_{47}Si_3Mn_{35}In_{15}$			
Atoms	Exp. Wt%	EDX Wt%	Wt% Diff.	Atoms	Exp. Wt%	EDX Wt%	Wt% Diff.
Ni	39.22	38.93	0.74	Ni	42.52	40.90	3.81
Mn	27.36	28.22	3.14	Mn	29.64	30.70	3.58
In	24.51	23.56	3.88	In	26.54	27.16	2.34
Bi	8.91	9.28	4.15	Si	1.30	1.24	4.62

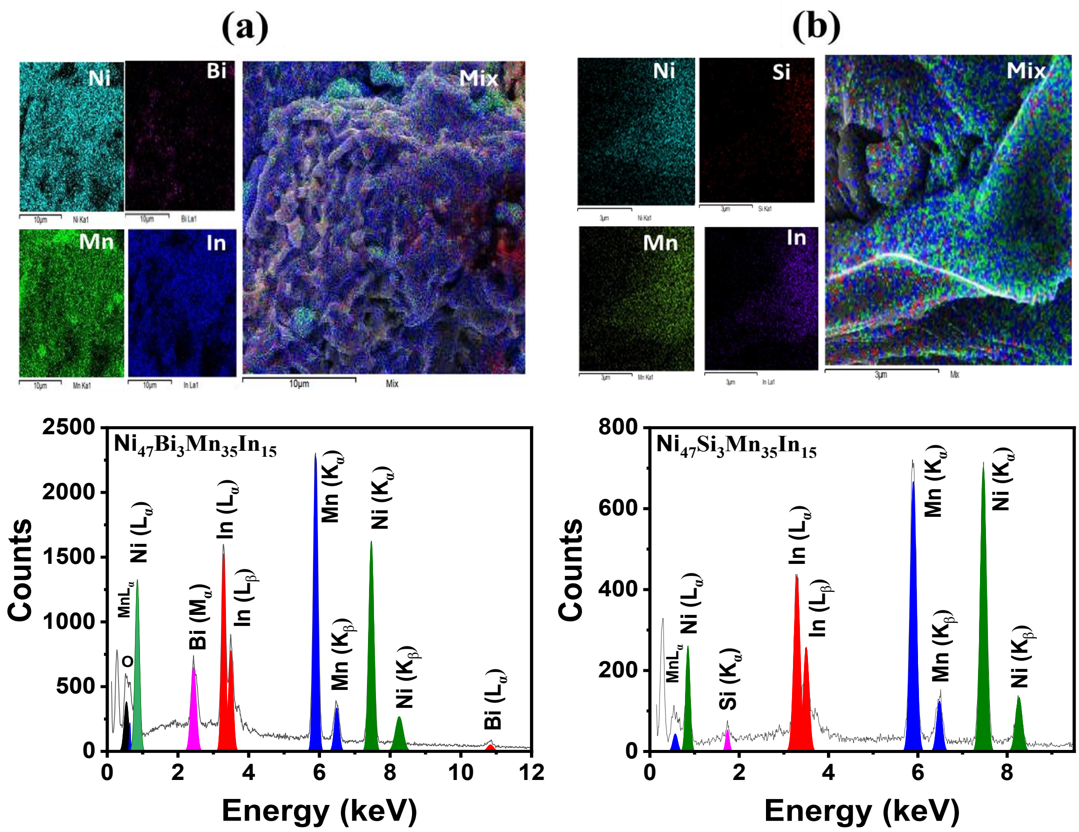

Figure 2. Scanning electron microscopy (SEM) image and elemental analysis by Energy Dispersive X-ray (EDX) spectrum for (a) $Ni_{47}Bi_3Mn_{35}In_{15}$ and (b) $Ni_{47}Si_3Mn_{35}In_{15}$.

Figure 3(a) and (b) show the temperature-dependent magnetization M(T) for $Ni_{47}Bi_3Mn_{35}In_{15}$ and $Ni_{47}Si_3Mn_{35}In_{15}$ measured under an applied field of H = 100 Oe using FCC and FCW protocols. For $Ni_{47}Bi_3Mn_{35}In_{15}$, a sharp change in magnetization is observed near the martensitic transition temperature (T_M), accompanied by pronounced thermal hysteresis, confirming a first-order phase transition (FOPT) from the ferromagnetic martensite phase to the ferromagnetic austenite phase [15,26]. Furthermore, a second-order transition from the ferromagnetic austenite to the paramagnetic phase is observed near the Curie temperature (T_C). The inset of Fig. 3(a) shows that increasing Bi concentration in $Ni_{50-x}Bi_xMn_{35}In_{15}$ (x = 0,1,3) leads to a decrease in T_C, bringing it closer to room temperature. This behavior is attributed to the substitution of non-magnetic Bi at the Ni site, which modifies the Mn–Mn interatomic distance and weakens the ferromagnetic exchange interactions, thereby reducing the overall magnetic coupling [27].

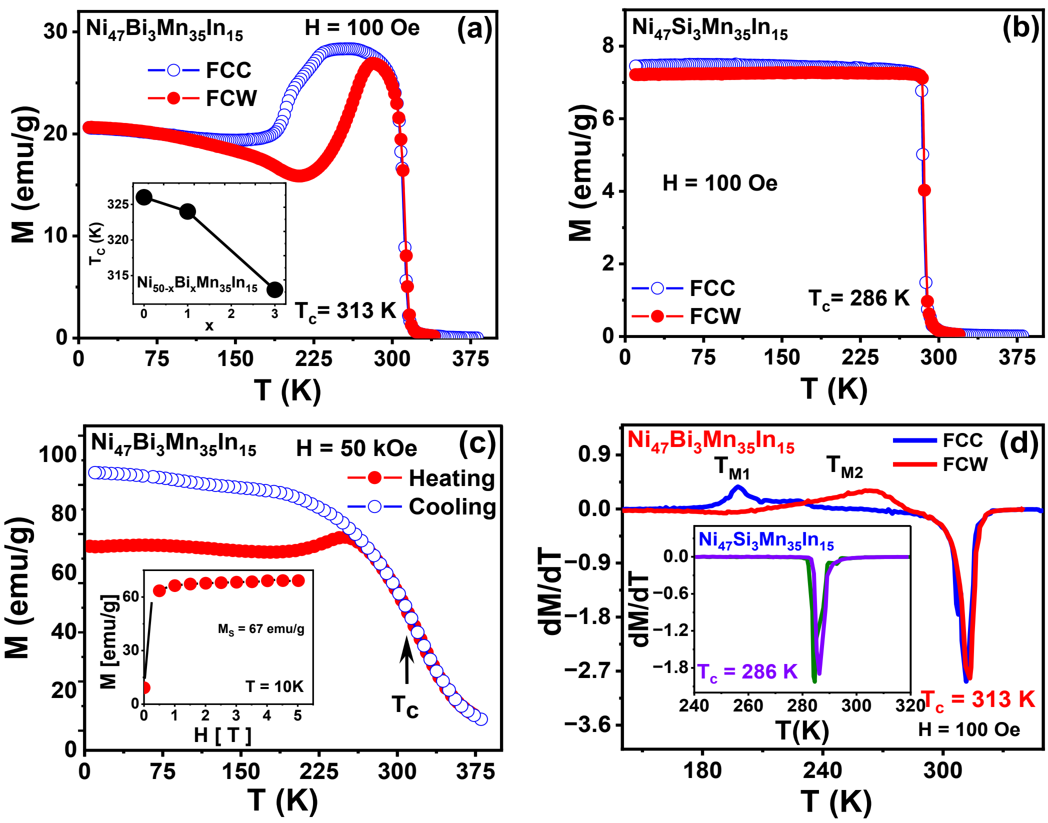

Figure 3. Temperature-dependent magnetization M(T) measured at H = 100 Oe for (a) Ni-Bi alloy, and (b) Ni-Si alloy. The inset in (a) shows the variation of Curie temperature (T_C) with Bi concentration in $Ni_{50-x}Bi_xMn_{35}In_{15}$ (x = 0, 1, 3). (c) M(T) curves measured at H = 50 kOe for Ni-Bi; the inset shows the corresponding M(H) curves at 10 K. (d) Temperature derivative of magnetization (dM/dT) as a function of temperature, used to estimate the magnetic transition temperatures; the inset shows dM/dT vs T for Ni-Si alloy.

In contrast, $Ni_{47}Si_3Mn_{35}In_{15}$ exhibits a single magnetic transition with nearly overlapping FCC and FCW curves, showing negligible thermal hysteresis (~1.8 K) and a predominantly second-order phase transition (SOPT), as further confirmed by the corresponding Arrott plots (Fig. 4 b). This suggests that Si substitution suppresses (or significantly weakens) the martensitic transformation and stabilizes the ferromagnetic austenitic phase. Owing to its smaller atomic size, Si induces lattice contraction, which reduces the Mn–Mn interatomic distance and alters the exchange interactions, favoring a more stable ferromagnetic state [26]. Previous studies have shown that Si substitution reduces the valence electron concentration (e/a ratio) and modifies the balance between ferromagnetic (FM) and antiferromagnetic (AFM) interactions through changes in Mn–Mn spacing, leading to a reduction in both magnetization and Curie temperature [28].

The magnetic behavior of these Heusler alloys is primarily governed by Mn atoms, whose large magnetic moments dominate the overall magnetization [28]. Due to the relatively large Mn–Mn separation, direct 3d–3d exchange is weak, and the magnetic interactions are mainly mediated by indirect Ruderman–Kittel–Kasuya–Yosida (RKKY)-type exchange [30]. Consequently, both Bi and Si substitutions influence the magnetic properties through modifications in lattice parameters, which directly tune the Mn–Mn exchange coupling and hence the observed magnetic transitions.

Figure 3(c) exhibits the M-T curves measured under an applied field of H = 50 kOe, which show that the first-order phase transition (FOPT) is significantly suppressed, as evidenced by the reduced hysteresis and the smoother nature of the transition. This weakening of the FOPT at higher field suggests field-induced stabilization of the ferromagnetic austenitic phase, consistent with previous findings [19,26]. The applied magnetic field favors the high-magnetization austenitic phase, thereby suppressing the low-magnetization martensitic phase due to the large difference in magnetization between the two phases [16,19]. The inset of Fig. 3(c) shows the M(H) curves at 10 K, where a saturation magnetization (M_S) of ~67 emu/g is observed for the Bi-substituted alloy, which is higher than that of the parent compound [19]. This enhancement suggests that Bi substitution enhances the overall magnetic response, likely through modification of Mn–Mn exchange interactions associated with lattice expansion.

The temperature dependence of the derivative of magnetization (dM/dT), shown in Figure 3(d), provides clear evidence for the coexistence of first-order and second-order magnetic phase transitions in $Ni_{47}Bi_3Mn_{35}In_{15}$. The dM/dT curves exhibit two anomalies T_{M1} and T_{M2} with clear thermal hysteresis between cooling and heating, confirming the first-order nature of the martensitic transition [19]. This behavior reflects abrupt changes in magnetization associated with a simultaneous structural transformation in the same temperature range. In contrast, near T_C = 313 K, the dM/dT curves exhibit a sharp minimum without any thermal hysteresis, characteristic of a second-order phase transition (SOPT). This is further supported by the Arrott plot shown in Fig. 4 (a). By contrast, the inset of Fig. 3(d) shows that the dM/dT curves for $Ni_{47}Si_3Mn_{35}In_{15}$ nearly overlap during cooling and heating over the full temperature range, indicating negligible thermal hysteresis and confirming a predominantly second-order transition. Unlike the Ni-Bi alloy, no low-temperature discontinuity is observed, suggesting the absence or strong suppression of the first-order transition in the Ni-Si alloy.

Figure 4 (a) and (b) show the Arrott plots for $Ni_{47}Bi_3Mn_{35}In_{15}$ and $Ni_{47}Si_3Mn_{35}In_{15}$, constructed using the mean-field approximation with critical exponents $\beta = 0.5$, and $\gamma = 1$. According to Banerjee's criterion, the positive slope of all isotherms confirms predominantly second-order nature of the magnetic phase transition near T_C in both alloys. Furthermore, the isotherm that passes closest to the origin corresponds to the Curie temperature (T_C), providing an independent estimation of the transition temperature [31]. From the combined analysis of the dM/dT vs T curves and the Arrott plots, the Curie temperatures of $Ni_{47}Bi_3Mn_{35}In_{15}$ and $Ni_{47}Si_3Mn_{35}In_{15}$ are determined to be 313 K and 286 K, respectively, in good agreement with the magnetization data.

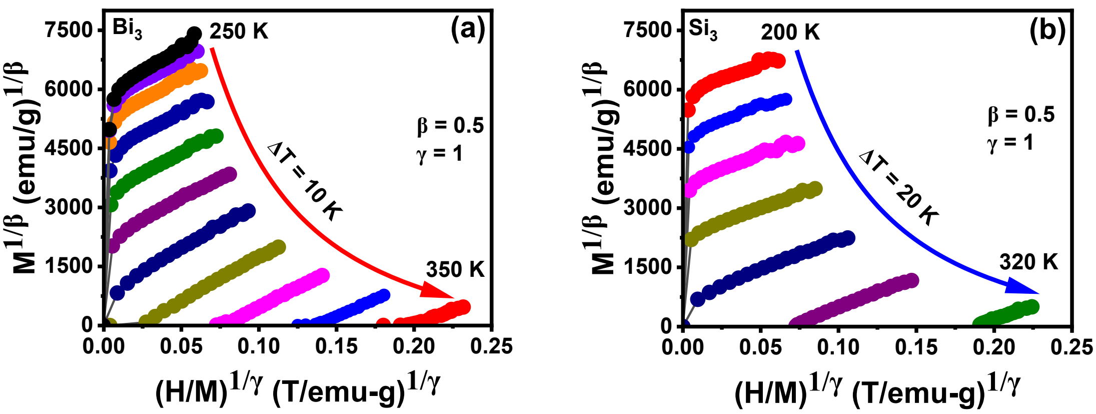

Figure 4. Arrott plots ($M^{1/\beta}$ vs H/M $^{1/\gamma}$) for (a) $Ni_{47}Bi_3Mn_{35}In_{15}$ and (b) $Ni_{47}Si_3Mn_{35}In_{15}$ measured in the vicinity of their second-order magnetic transition.

Figure 5 (a) and (b) show the isothermal magnetization [M(H)] curves for $Ni_{47}Bi3Mn_{35}In_{15}$ and $Ni_{47}Si3Mn_{35}In_{15,}$ respectively measured over selected temperature ranges with intervals of ΔT = 10 K and 20 K under an applied magnetic field of up to 50 kOe. Figure 5 (c) and (d) present the corresponding magnetic entropy changes ($|\Delta S_M|$) as a function of temperature for both alloys, estimated from the M(H) data using Maxwell's thermodynamic relation under a magnetic field change of ΔH = 5 T [3,6]. Magnetocaloric properties are primarily evaluated near the second-order transition region due to its reversible nature and negligible hysteresis. Previuosly, $Ni_{49}BiMn_{35}In_{15}$ was reported to exhibit a maximum magnetic entropy change of $|\Delta S_M|$ = 5.5 $Jkg^{-1}K^{-1}$ and relative cooling power of 312 Jkg^{-1} at T_C = 325 K. In the present study, increasing the Bi-content leads to an enhanced

 doi:10.20944/preprints202604.0708.v1

magnetocaloric response, with |ΔSM| = 6 Jkg⁻¹K⁻¹ and RCP and refrigerant capacity (RC) values of 303 Jkg⁻¹ and 257 Jkg⁻¹, respectively. In contrast, substitution with 3 at.% Si reduces the magnetic entropy change to |ΔSM| = 4.2 Jkg⁻¹K⁻¹, while the RCP increases to 345 Jkg⁻¹ (RC = 300 Jkg⁻¹) at T_C = 286 K. The enhanced magnetocaloric response in the Ni–Bi alloy is attributed to lattice expansion, which increases the Mn–Mn interatomic distance and enhances the magnetization change across the transition [19]. In contrast, Si substitution induces lattice contraction, reducing the Mn–Mn distance and modifying the balance between ferromagnetic (FM) and antiferromagnetic (AFM) interactions, thereby lowering |ΔSM|. However, the relatively higher RCP (and RC) values observed for the Si-substituted alloy arise from the broader |ΔSM|-T peak, which extends the effective temperature span of the magnetocaloric response [22,28]. These parameters represent key figures of merit for magnetic refrigeration, reflecting the heat transfer capability between the hot and cold reservoirs during a magnetic refrigeration cycle, and are widely used to evaluate material performance [16,19]. Furthermore, previous studies have show that doping Ni-Mn-In alloys with magnetic elements such as Cu, Co, Fe, and Mn enhances |ΔSM|, due to the strengthening of magnetic exchange interactions, particularly Mn-Mn and Ni-Mn coupling [26].

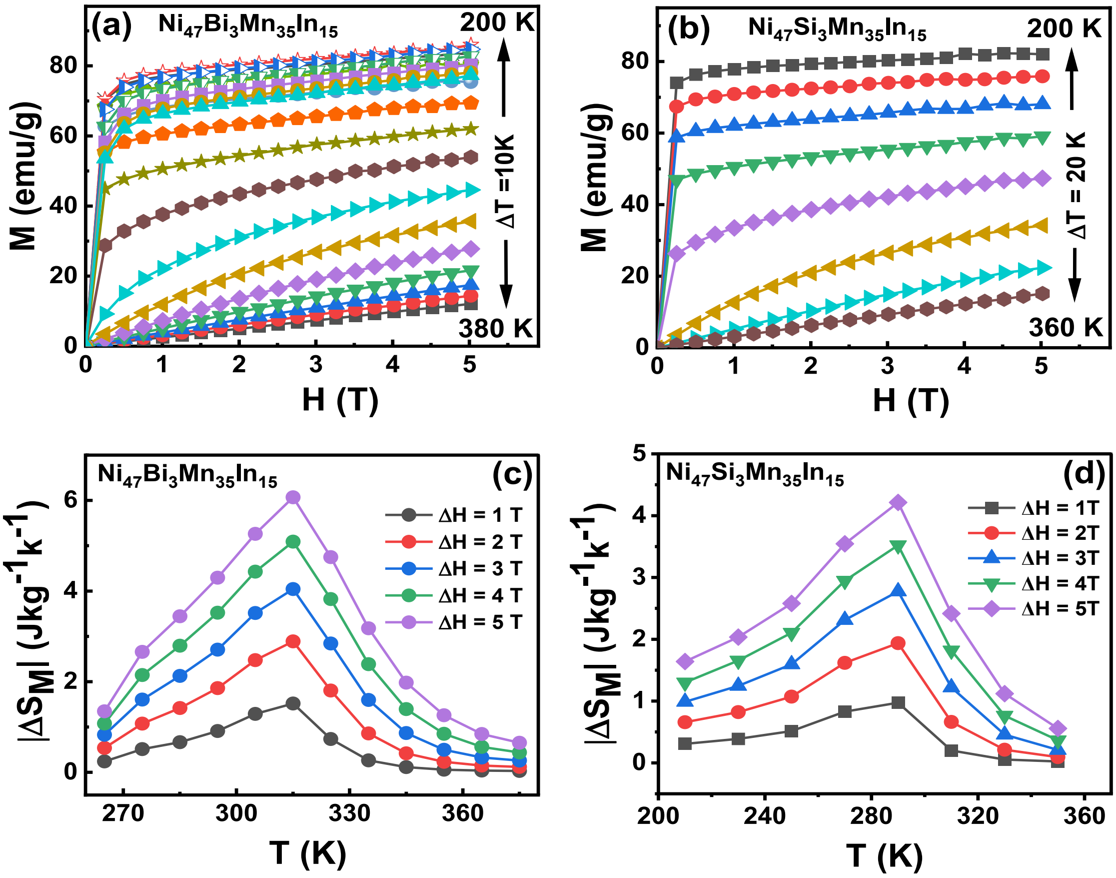

Figure 5. (a) and (b) Isothermal magnetization curves M(H) measured at selected temperatures under varying magnetic fields. (c) and (d) Corresponding magnetic entropy change |ΔSM| derived from the isothermal magnetization curves (M(H)) for a magnetic field change of ΔH=50 kOe.

Figure 6 (a) exhibits the comparison of magnetic entropy change (|ΔSM|) for both alloys under different magnetic field changes (ΔH = 1- 5 T). The inset of Fig. 6(a) shows the relative cooling power for both alloys evaluated at ΔH = 5 T. Although, the magnetic entropy change (|ΔSM|) is lower than that reported for some Ni–Mn-based Heusler alloys, the present systems exhibits a broader magnetic transition, resulting in a competitive relative cooling power (RCP), thereby enhancing their suitability for practical magnetic refrigeration [3,9]. It is also noteworthy that several compositions listed in

 doi:10.20944/preprints202604.0708.v1

Table 2 exhibit lower |ΔS_M| values than the present systems, thereby highlighting the competitive overall magnetocaloric performance achieved in this study.

Figure 6 (b) shows the temperature-dependent resistivity (ϱ) of $Ni_{47}Bi_3Mn_{35}In_{15}$ at zero field, along with the magnetic susceptibility (χ) measured under an applied field of 100 Oe during cooling. The resistivity was calculated from four-probe resistance measurements using $\varrho = (R * A)/L$, where A is the cross-sectional area and L is the distance between voltage contacts. Two distinct transitions are observed: (i) a sharp drop in resistivity near T_M, indicating a first-order martensitic transformation, and (ii) a gradual change in slope near T_C, corresponding to a second-order ferromagnetic-paramagnetic transition associated with spin disorder scattering [16]. These features are consistent with the corresponding χ(T) data and are in good agreement with previous reports on Ni-Mn-based Heusler alloys [32–34].

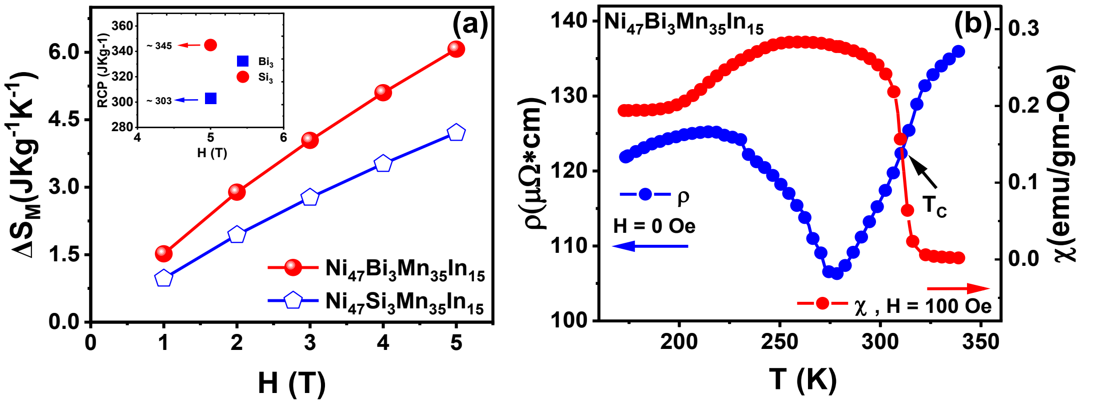

Figure 6. (a) Comparison of magnetic entropy change (ΔS_M) for $Ni_{47}Bi3Mn_{35}In_{15}$ and $Ni_{47}Si_3Mn_{35}In_{15}$ alloys under different magnetic field changes (1 T -5 T). (b) Temperature dependence of resistivity and DC magnetic susceptibility of the $Ni_{47}Bi_3Mn_{35}In_{15}$ sample. The inset in (a) shows the relative cooling power (RCP) for both alloys estimated at a magnetic field change of 5 T field.

Table 2. Comparison of magnetic entropy changes |ΔS_M| and relative cooling power (RCP) for representative Heusler alloys in the vicinity of the second-order phase transition (SOPT) under an applied magnetic field change of ΔH = 5 T.

S.N.	Systems	|ΔS_M| [$JKg^{-1}K^{-1}$]	RCP [JKg^{-1}]	T_C [K]	References
1.	$Ni_{47}Bi_3Mn_{35}In_{15}$	6	303	313	This work
2.	$Ni_{47}Si_3Mn_{35}In_{15}$	4.2	345	286	This work
3.	$(Ni_{37.5}Co_{12.5}Mn_{35}Ti_{15})_{99.9}B_{0.4}$	12.2	183	305	[35]
4.	$Ni_{50}Mn_{34.80}In_{15.2}$	7	224	328	[22]
5.	$Ni_{49}Mn_{35}In_{15}Bi$	5.5	312	325	[16]
6.	$Ni_{50}Mn_{35}In_{14.50}Bi_{0.5}$	5	165	320	[19]
7.	$Ni_{45}Co_5Mn_{37.5}In_{12.5}$	20	-	368	[26]
8.	$Ni_2Mn_{0.75}Cu_{0.25}Ga$	65	-	308	[20]
9.	$Ni_{52}Mn_{26}Ga_{22}$	11.4	-	348	[36]
10.	$Ni_{50}Mn_{35}In_{15}$	5.4	-	324	[19]
11.	$Ni_{44}Mn_{36}In_{14}Co_6$	23.5	250	368	[37]
12.	$Ni_{47}Cu_2Mn_{38}Sn_{13}$	3.54	-	316	[38]
13.	$Ni_2Mn_{1.34}In_{0.66}$	4.5	201	305	[30]
14.	$Ni_{42}Mn_{46}CoSn_{11}$	0.97	129	350	[39]
15.	$Ni_{50}Mn_{35}In_{10}Fe_5$	1.4	74	298	[40]
16.	$Ni_{50}Mn_{32}Sn_{10}Fe_8$	10.04	184	318	[41]

17.	$MnNi_{0.85}Fe_{0.15}Ge$	4.88	36.33	274	[29]
18.	$Mn_{70}Ni_{25}Ga_5$	12.48	91.38	322	[42]
19.	$Ni_{50}Mn_{34}In_{15.5}Al_{0.5}$	3.86	9.9	321	[43]
20.	$Ni_{36}Co_{14}Mn_{35}Ti_{15}$	~20	~285	305	[44]

Conclusions

In summary, we have investigated the structural, magnetic, magnetocaloric, and magneto-transport properties of Ni–Mn–In-based Heusler alloys with partial substitution of Ni by Bi and Si (3 at.%). A clear contrasting behavior is observed between Bi and Si substitution. Bi substitution enhances magnetocaloric performance, with the maximum magnetic entropy change ($|\Delta S_M|$) increasing from 5.5 to 6 J kg^{-1} K^{-1} as the Bi content increases from 1 to 3 at.%. In contrast, Si substitution leads to a reduction in $|\Delta S_M|$, while the broadening of the ΔS_M peak results in an enhanced RCP. Furthermore, the Curie temperatures of both alloys (286 K and 313 K) lie near room temperature (~300 K), which is desirable for practical magnetocaloric applications. These results demonstrate that lattice expansion (Bi) and contraction (Si) distinctly modify Mn–Mn exchange interactions, thereby governing the magnetocaloric response. These contrasting trends highlight the distinct roles of Bi and Si substitution in tuning the magnetocaloric response of Ni–Mn–In-based Heusler alloys.

Acknowledgments: N. Ali: I. Dubenko, S. Talapatra, and A. Oli acknowledges support from the U.S. Department of Energy (DOE), Office of Basic Energy Sciences under Award No. DE-FG02-06ER46291. S. Stadler acknowledges support from the U.S. Department of Energy (Grant No., DE-SC00-10521).

References

1. C. Maji, "Heusler Alloys: Sustainable Material for Sustainable Magnetic Refrigeration," Handbook of Sustainable Materials: Modelling, Characterization, and Optimization, pp. 323–339, Jan. 2023, doi: 10.1201/9781003297772-17
2. A. B. Batdalov et al., "Magnetic, thermal, and electrical properties of an $Ni_{45.37}Mn_{40.91}In_{13.72}$ Heusler alloy," Journal of Experimental and Theoretical Physics, vol. 122, no. 5, pp. 874–882, May 2016, doi: 10.1134/S1063776116040129/METRICS.
3. A. Oli et al., "Effects of carbon substitution on magnetic properties and magnetocaloric effects in $Mn_{65-x}Ga_{17}C_{18+x}$ compounds," J. Alloys Compd., vol. 1017, p. 179036, Feb. 2025, doi: 10.1016/J.JALLCOM.2025.179036.
4. N. Tiwari et al., "Manganese- Copper- Gallium Alloys for Sustainable Refrigeration Through a Synergistic Study of Magnetocaloric and Mechanical Behavior," Adv. Eng. Mater., Mar. 2026, doi: 10.1002/ADEM.202502236.
5. M. Shahbazi, A. Dehghan Manshadi, K. Shinde, and I. D. R. Mackinnon, "Magnetocaloric Properties and Microstructures of HoB_2 and Nb-Substituted HoB_2," Materials, vol. 18, no. 4, Feb. 2025, doi: 10.3390/MA18040866/S1.
6. A. Wederni, J. Daza, W. Ben Mbarek, J. Saurina, L. Escoda, and J. J. Suñol, "Crystal Structure and Properties of Heusler Alloys: A Comprehensive Review," Metals (Basel)., vol. 14, no. 6, Jun. 2024, doi: 10.3390/MET14060688.
7. E. Villa et al., "Shape memory and elastocaloric properties of melt-spun NiMn-based Heusler alloys," J. Alloys Compd., vol. 965, p. 171437, Nov. 2023, doi: 10.1016/J.JALLCOM.2023.171437.
8. P. Sivaprakash, I. Kim, S. Divya, S. Hajra, T. H. Oh, and S. Esakki Muthu, "Influence of non-magnetic Cu on structural, magnetic and magnetocaloric properties on NiMnIn bulk Heusler alloys," Materials Science and Engineering: B, vol. 297, p. 116760, Nov. 2023, doi: 10.1016/J.MSEB.2023.116760.
9. A. Oli, I. Dubenko, et al., "Investigation of Phase Transitions, Magnetic Properties and Magnetocaloric effect in $Mn_{60}Ga_{20-x}In_xC_{20}$ (x= 1, 2, 3, 4, 5) by the partial substitution of In in Ga". In *SMT conference 2025*.
10. C. Felser, "Heusler Alloys: Properties, Growth, and Applications," in Heusler Alloys, Springer, p. 168, 2016.

11. A. Gschneidner, V. K. Pecharsky, and A. O. Tsokol, "Recent developments in magnetocaloric materials," Reports on Progress in Physics, vol. 68, no. 6, p. 1479, May 2005, doi: 10.1088/0034-4885/68/6/R04.
12. B. Beckmann et al., "Giant magnetocaloric effect of Ni-Co-Mn-Ti all-d Heusler alloys in high magnetic fields," Acta Mater., vol. 282, p. 120460, Jan. 2025, doi: 10.1016/J.ACTAMAT.2024.120460.
13. X. Zhang, Z. Guo, F. Zhang, and Y. Li, "Recent Advances in Magnetocaloric Effect of High-Entropy Alloys," Coatings 2025, Vol. 15, vol. 15, no. 12, Dec. 2025, doi: 10.3390/COATINGS15121425.
14. S. Karki Chhetri et al., "Large negative magnetoresistance in antiferromagnetic Gd_2Se_3," Phys. Rev. B, vol. 111, no. 1, p. 014431, Jan. 2025, doi:10.1103/PHYSREVB.111.014431
15. A. Aryal, I. Dubenko, A. Granovsky, and E. Lähderanta, "Magnetic field dependence of the martensitic transition and magnetocaloric effects in $Ni_{49}BiMn_{35}In_{15}$," 2020, doi: 10.1063/1.5130405.
16. I. Dubenko et al., "Comparing magnetostructural transitions in $Ni_{50}Mn_{18.75}Cu_{6.25}Ga_{25}$ and $Ni_{49.80}Mn_{34.66}In_{15.54}$ Heusler alloys," J. Magn. Magn. Mater., vol. 401, pp. 1145–1149, Mar. 2016, doi: 10.1016/J.JMMM.2015.11.025.
17. A. Oli et al., "Phase Transitions and Magnetocaloric Effects in $Ni_{50}Mn_{35}In_{12}Bi_3$ and $Ni_{47}Bi_3Mn_{35}In_{15}$ Heusler Alloys," APS, vol. 2023, p. Z54.008, 2023, Accessed: Feb. 22, 2026. https://ui.adsabs.harvard.edu/abs/2023APS..MARZ54008O/abstract
18. A. Aryal et al., Effect of Bi substitution on the magnetic and magnetocaloric properties of $Ni_{50}Mn_{35}In_{15-x}Bi_x$ Heusler alloys," AIP Adv., vol. 8, p. 56409, 2018, doi: 10.1063/1.5004694.
19. S. Stadler, M. Khan, J. Mitchell, N. Ali, and A. M. Gomes, "Magnetocaloric Properties of $Ni_2Mn_{1-x}Cu_xGa$," Physics Published in Applied Physics Letters, vol. 88, no. 19, 2006, doi: 10.1063/1.2202751.
20. I. Dubenko, A. Oli, et al., "Magnetic properties of B doped Mn-Ga-C based alloys," J. Magn. Magn. Mater., p. 171505, Nov. 2023, doi: 10.1016/J.JMMM.2023.171505.
21. A. K. Pathak, M. Khan, I. Dubenko, S. Stadler, and N. Ali, "Large magnetic entropy change in $Ni_{50}Mn_{50-x}In_x$ Heusler alloys," Appl. Phys. Lett., vol. 90, no. 26, p. 262504, Jun. 2007, doi: 10.1063/1.2752720/333732.
22. L. Chen et al., "Magnetoresistance and magnetocaloric properties involving strong metamagnetic behavior in Fe-doped $Ni_{45}(Co_{1-x}Fe_x)_5Mn_{36.6}In_{13.4}$ alloys," Appl. Phys. Lett., vol. 101, no. 1, p. 12401, Jul. 2012, doi: 10.1063/1.4732525/126430.
23. D. Bourgault, J. Tillier, P. Courtois, D. Maillard, and X. Chaud, "Large inverse magnetocaloric effect in $Ni_{45}Co_5Mn_{37.5}In_{12.5}$ single crystal above 300 K," Appl. Phys. Lett., vol. 96, no. 13, p. 132501, Mar. 2010, doi: 10.1063/1.3372633/892475.
24. P. Ari-Gur et al., "The use of diffraction techniques for understanding structure–property relationships in Heusler alloys," J. Magn. Magn. Mater., vol. 596, p. 171809, Apr. 2024, doi: 10.1016/J.JMMM.2024.171809.
25. A. K. Pathak, I. Dubenko, Y. Xiong, P. W. Adams, S. Stadler, and N. Ali, "Effect of partial substitution of Ni by Co on the magnetic and magnetocaloric properties of $Ni_{50}Mn_{35}In_{15}$ Heusler alloy," J. Appl. Phys., vol. 109, no. 7, Apr. 2011, doi: 10.1063/1.3540696/977023.
26. J. R. Ares, A. Pascual, I. J. Ferrer, and C. Sánchez, "A methodology to reduce error sources in the determination of thin film chemical composition by EDAX," Thin Solid Films, vol. 450, no. 1, pp. 207–210, Feb. 2004, doi: 10.1016/J.TSF.2003.10.073.
27. K. Ahn, "Ni-Mn based conventional full Heusler alloys, all-d-metal full Heusler alloys, and their promising functional properties to solid state cooling by magnetocaloric effect," J. Alloys Compd., vol. 978, p. 173378, Mar. 2024, doi: 10.1016/J.JALLCOM.2023.173378.
28. B. Boussaida and R. Masrour, "Electronic structure, magnetic properties, and magnetocaloric performance of $MnNi_{1-x}Fe_xGe$ (x = 0.15 and 0.18) alloys: A combined KKR-CPA and Monte Carlo study," Mater. Chem. Phys., vol. 358, p. 132370, Jun. 2026, doi: 10.1016/J.MATCHEMPHYS.2026.132370.
29. B. Dahal et al., "Effect of partial substitution of in with Mn on the structural, magnetic, and magnetocaloric properties of $Ni_2Mn_{1+x}In_{1-x}$ Heusler alloys," J. Phys. D Appl. Phys., vol. 52, no. 42, Aug. 2019, doi: 10.1088/1361-6463/AB335A.
30. B. K. Banerjee, "On a generalised approach to first and second order magnetic transitions," Physics Letters, vol. 12, no. 1, pp. 16–17, Sep. 1964, doi: 10.1016/0031-9163(64)91158-8.

 doi:10.20944/preprints202604.0708.v1

31. H. Kerrai, H. Saadi, E. M. Jalal, M. Kerouad, and A. Zaim, "Hysteresis behavior and magnetocaloric effect in $MnNiGa_2$ full-Heusler alloy," Solid State Commun., vol. 394, p. 115717, Dec. 2024, doi: 10.1016/J.SSC.2024.115717.
32. A. P. Kamantsev et al., "Inverse Magnetocaloric Effect in Heusler $Ni_{44.4}Mn_{36.2}Sn_{14.9}Cu_{4.5}$ Alloy at Low Temperatures," Metals 2023, Vol. 13, Page 1985, vol. 13, no. 12, p. 1985, Dec. 2023, doi: 10.3390/MET13121985.
33. D. Bourgault, L. Porcar, S. Rivoirard, P. Courtois, and V. Hardy, "Entropy change of a $Ni_{45.5}Co_{4.5}Mn_{37}In_{13}$ single crystal studied by scanning calorimetry in high magnetic fields: Field dependence of the magnetocaloric effect," Appl. Phys. Lett., vol. 107, no. 9, Aug. 2015, doi: 10.1063/1.4929950.
34. M. López-Cruz, R. Varga, and J. L. Sánchez Llamazares, "Magnetostructural Transformation and Magnetocaloric Properties of $(Ni_{37.5}Co_{12.5}Mn_{35}Ti_{15})_{100-x}B_x$ (x = 0.0 and 0.4) Melt-Spun Ribbons," Metals (Basel)., vol. 14, no. 2, p. 216, Feb. 2024, doi: 10.3390/MET14020216/S1.
35. Z. B. Li et al., "Microstructure and magnetocaloric effect of melt-spun $Ni_{52}Mn_{26}Ga_{22}$ ribbon," Appl. Phys. Lett., vol. 100, no. 17, p. 174102, Apr. 2012, doi: 10.1063/1.4704780/384991.
36. Z. N. Zhou et al., "Tuning martensite transformation behavior and magneto-caloric effect in $Ni_{44}Mn_{36}In_{14}Co_6$ alloy through doping the fifth element Cu," J. Alloys Compd., vol. 817, p. 153150, Mar. 2020, doi: 10.1016/J.JALLCOM.2019.153150.
37. S. Paramasivam, E. M. Sankaran, and I. Kim, "Investigation of magnetic, magnetocaloric cooling, magneto transport properties and critical behavior of Cu-doped $Ni_{49}Mn_{38}Sn_{13}$ alloys," J. Magn. Magn. Mater., vol. 614, p. 172737, Feb. 2025, doi: 10.1016/J.JMMM.2024.172737.
38. K. Dadda, L. Ghouari, A. Elmohri, M. Y. Debili, and E.-K. Hlil, "Prediction of the Magnetocaloric Effect of $Ni_{42}Mn_{46}CoSn_{11}$ Heusler Alloy with a Phenomenological Model," Materials Proceedings 2025, Vol. 25, vol. 25, no. 1, p. 4, Nov. 2025, doi: 10.3390/MATERPROC2025025004.
39. T. Bachagha, R. Chakaravarthy, W. Ren, J. Saurina, and J. J. Suñol, "Structural, Magnetocaloric, and Magnetic Properties in Heusler $Ni_{50}Mn_{35}In_{10}X_5$ (X = Ga, Fe and Al) Alloys," Metals 2023, Vol. 13, vol. 13, no. 12, Nov. 2023, doi: 10.3390/MET13121913.
40. R. Li, P. K. Liaw, J. Jiang, L. Deng, and Y. Zhang, "Design strategy for enhancing mechanical properties and magnetocaloric effect of eutectic Ni-Mn-Sn-Fe alloy via laser powder bed fusion," Materials Science and Engineering: A, vol. 954, p. 149795, Feb. 2026, doi: 10.1016/J.MSEA.2026.149795.
41. N. Tiwari et al., "Magnetocaloric Effect in Mn-rich Heusler derived Alloys for Room Temperature Application". J. Mater. Chem. C, vol. 13, p. 10789, 2025, doi: 10.1039/d4tc04242e
42. M. Arman, F. Shahri, R. Gholamipour, and S. Sohrabi, "Effect of Al doping on the magnetic, magneto-structural, and magnetocaloric properties of Ni-Mn-In Heusler alloys," 2024, doi: 10.1016/j.ssc.2024.115767.
43. A. N. Khan et al., "Enhanced local homogeneity obtained by induction melting for optimizing reversible magnetocaloric response in all-d-metal Ni(Co)-Mn-Ti Heusler alloys," J. Alloys Compd., vol. 1052, p. 186135, Jan. 2026, doi: 10.1016/J.JALLCOM.2026.186135.